



LAWRENCE
LIVERMORE
NATIONAL
LABORATORY

Demonstration of enhanced DQE with a dual MCP configuration

N. Izumi, G. N. Hall, A. C. Carpenter, F. V. Allen, J. G. Cruz, B. Felker, D. Hargrove, J. Holder, J. D. Kilkenny, A. Lombard, R. Montesanti, N. E. Palmer, K. Piston, G. Stone, M. Thao, R. Vern, R. Zacharias, O. L. Landen, R. Tommasini, D. K. Bradley, P. M. Bell

September 23, 2014

SPIE 2014
San Diego, CA, United States
August 17, 2014 through August 21, 2014

Disclaimer

This document was prepared as an account of work sponsored by an agency of the United States government. Neither the United States government nor Lawrence Livermore National Security, LLC, nor any of their employees makes any warranty, expressed or implied, or assumes any legal liability or responsibility for the accuracy, completeness, or usefulness of any information, apparatus, product, or process disclosed, or represents that its use would not infringe privately owned rights. Reference herein to any specific commercial product, process, or service by trade name, trademark, manufacturer, or otherwise does not necessarily constitute or imply its endorsement, recommendation, or favoring by the United States government or Lawrence Livermore National Security, LLC. The views and opinions of authors expressed herein do not necessarily state or reflect those of the United States government or Lawrence Livermore National Security, LLC, and shall not be used for advertising or product endorsement purposes.

Demonstration of enhanced DQE with a dual MCP configuration

N. Izumi*^a, G. N. Hall^a, A. C. Carpenter^a, F. V. Allen^a, J. G. Cruz^a, B. Felker^a, D. Hargrove^a, J. Holder^a, J. D. Kilkenny^b, A. Lumbard^a, R. Montesanti^a, N. E. Palmer^a, K. Piston^a, G. Stone^a, M. Thao^a, R. Vern^a, R. Zacharias^a, O. L. Landen^a, R. Tommasini^a, D. K. Bradley^a and P. M. Bell.

^aLawrence Livermore National Laboratory, Livermore, CA 94550

^bGeneral Atomics, 3550 General Atomics Court, San Diego, CA 92121

ABSTRACT

X-ray framing cameras based on proximity-focused micro-channel plates (MCP) have been playing an important role as diagnostics of inertial confinement fusion experiments [1]. Most of the current x-ray framing cameras consist of a single MCP, a phosphor, and a recording device (e.g. CCD or photographic films). This configuration is successful for imaging x-rays with energies below 20 keV, but detective quantum efficiency (DQE) above 20 keV is severely reduced due to the large gain differential between the top and the bottom of the plate for these volumetrically absorbed photons [2]. Recently developed diagnostic techniques at LLNL require recording backlit images of extremely dense imploded plasmas using hard x-rays, and demand the detector to be sensitive to photons with energies higher than 40 keV [3]. To increase the sensitivity in the high-energy region, we propose to use a combination of two MCPs. The first MCP is operated in low gain and works as a thick photocathode, and the second MCP works as a high gain electron multiplier [4,5]. We assembled a proof-of-principle test module by using this dual MCP configuration and demonstrated 4.5% DQE at 60 keV x-rays.

Keywords: gated x-ray imager, x-ray framing camera, Compton radiography, micro-channel plate

INTRODUCTION

Because of its strong intensity and excellent timing performance, laser-produced plasma x-ray sources have been used in various inertial confinement fusion experiments [6-13]. A X-ray radiography based on a photoelectric absorption in the imploding ablator region (~500 ps before the maximum x-ray self-emission from the core) has successfully been providing useful information about the symmetry of the implosion experiments [13]. However, due to strong self-emission from the hot core region, the radiography based on photoelectric absorption in the shell (x-ray energy 6 ~ 20 keV) is difficult when approaching the time of peak in the x-ray self-emission. Recently developed high-energy point-source radiography based on Compton scattering (Compton Radiography) is a promising way to observe assembly of the high-density fuel near the maximum compression time [3]. When the photon energy of the backlight source is higher than 40 keV, Compton scattering dominates the interaction of photons with the object. Due to the relatively flat cross section (~0.6 barn or less), Compton radiography provides an almost ideal and photon-energy independent contrast (transmission ~ 1/e) for highly compressed DT fuel (areal density ~1000 mg/cm²) and allows the use of a broadband x-ray source from Bremsstrahlung (40 ~200 keV, which is more than 10 times brighter than laser produced K line sources). Because of the point projection geometry used, as opposed to using pinholes for imaging, the self-emission x-ray from the compressed core casts a uniform background on the radiograph. By using relatively thick x-ray filters (for example Cu 100 ~500μm) it is possible to suppress the background due to self-emission x-ray from the core plasma.

However, in order to implement this Compton radiography at the National Ignition Facility, we need a new gated imaging detector which has good performance for 40 ~200 keV x-rays. Historically, we have been using proximity-focused MCP based x-ray framing cameras [1]. Most of current MCP based cameras have a single MCP. Those cameras with single MCP have excellent performance below 20 keV, but becomes noisy for x-rays over 30 keV.

In an MCP detector, incoming x-ray photons are converted to primary electrons, and those primary electrons produce secondary electrons inside the MCP material (lead glass). Some fraction of secondary electrons produced in an escape depth ($L_s \sim 33\text{\AA}$) has a chance to be released into the pores, accelerated by the electric field, and get amplified while

colliding many times on the pore walls (avalanche amplification). Therefore the single MCP is working as both a photocathode and an amplifier.

Generally speaking, detectors using avalanche amplification have noise due to the stochastic behavior of the amplification (avalanche noise) [14]. In the case of x-ray detection, the avalanche noise is significant because most of avalanche streams are starting from just a few secondary electrons.

The other noise source is a depth dependent amplification gain. In the case of low energy x-ray (< 5keV), most of x-ray photons are absorbed on the pore wall directly seen by the x-ray source (0 ~ 72μm from the irradiated surface of the plate). However, when x-ray energy is more than 30 keV, the mean-free-path of x-rays exceeds the thickness of the MCP (~70 mg/cm²) and incoming x-rays volumetrically excite the MCP. The avalanche stream events started near the entrance experience large gain while deep events experience small gain. This depth dependent gain is significant when the MCP is operated in the high gain regime [15].

In order to reduce the noise due to this depth dependent gain effect, we propose to stack two MCPs. The first one is operated in low-gain and works as a thick photocathode. The second one operates in high gain mode and works as an electron multiplier. By separating the photocathode from the amplifier, it is possible to suppress the noise due to depth dependence gain while keeping the required total gain of the system.

QUANTUM EFFICIENCY OF MCP AS A STRUCTURED PHOTOCATHODE

Quantum efficiency (QE) is defined as the ratio of the number of the detected events per the number of incident photons.

$$QE \equiv \frac{N_{detected_events}}{N_{incident_photons}} \quad (1)$$

In an MCP, x-ray photons are converted to primary electrons first. Those primary electrons excite the material (lead glass) and generate secondary electrons. A fraction of secondary electrons produced near the pore wall surface can escape into the pore and initiate the avalanche stream. To estimate the spectrum dependent quantum efficiency, it is important to model the transport of x-ray (incident, florescence, and blemsstrahlung), primary electrons (via photoelectric, Auger, and Compton), and the sedoncary electrons in the MCP material. We estimated the quantum efficiency of the MCPs by using Monte Carlo simulation MCNP6 [16]. The photon transport was calculated by Monte Carlo method. The primary and secondary electrons down to 20eV was calculated with condensed history method. However, this 20 eV cut-off energy is not low enough to directly calculate the number of secondaries escaped into the pore (N_s). Therefore, we estimated N_s by using an empirical model based on energy deposition in the pore wall surface [17],

$$N_s = \frac{P_s}{\varepsilon} \int \frac{dE(z)}{dz} \exp\left(-\frac{z}{L_s}\right) dz \quad (2)$$

where dE/dz is the energy deposited in depth z from the pore surface calculated by MCNP6, L_s is the average escape length of the secondary electrons, ε is the energy required to produce an internal secondary electron, and P_s is the possiblility that an electron at the surface can escape into the pore. Table 1 summarizes the parameters assumed in this calculation. All the events which generated more than 1 secondary electron into the pore was counted as one detected event.

Table 1. Parameters assumed in the calculation of secondary electron production

Parameters	Value
ϵ	10 eV
P_s	0.15
L_s	33 Angstrom

Fig. 1 shows the calculated QE for two different MCPs (thickness L: 460 μm and 800 μm). Both of them have the same pore diameter (10 μm), interval (12 μm), and offset angle (8 deg). When x-ray energy is lower than 5 keV, they have identical QE because all the photons are absorbed in the 1st wall directly seen by the source. The QE over 5 keV is increasing again because the x-rays penetrate through the 1st pore wall and has a chance to generate the secondary electrons on the 2nd pore wall. When the primary electron energy exceeds ~ 25 keV, they penetrate through the pore wall and have a chance to generate secondary electrons on the surface of adjacent pores. Because of the higher QE, we decided to use 800 μm thick MCP as the photocathode.

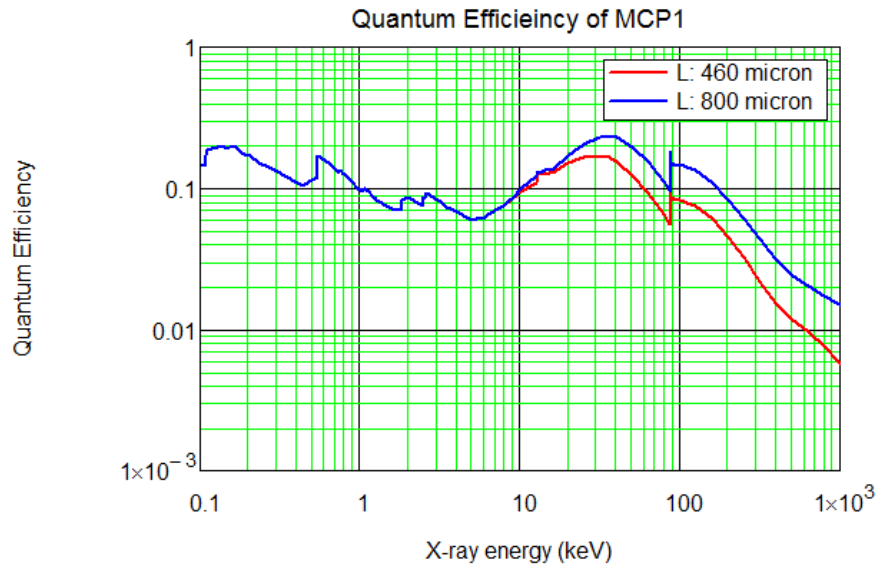


Fig. 1. QE of the MCPs calculated with Monte Carlo simulations. The expected reduction of QE due to termination of the avalanche stream in the pore is not included. Lower QE is expected when the MCP is operated in low gain regime.

DQE AND NOISE FACTOR

The QE is commonly used for evaluation of the signal-to-noise ratio of the obtainable image of detectors which have narrow pulse height distribution (PHD) (e.g., charge-coupled device or high-purity germanium detectors). For detectors, which have avalanche noise and broad PHD, detective quantum efficiency (DQE) is the quantity of interest [18]

$$DQE \equiv \left(\frac{SNR_{out}}{SNR_{in}} \right)^2, \quad (3)$$

where SNR_{out} and SNR_{in} are signal-to-noise ratio of output and input of the detector, respectively. When the statistical behavior of the input photons follows Poisson statistics, the expected signal-to-noise ratio of the image can be evaluated as

$$SNR_{out} = \sqrt{DQE \times N_i} \quad (4),$$

where N_i is the number of incident photons per resolution element.

Another useful metric of the loss of the available information caused by the statistical fluctuation of the avalanche process is the noise factor NF defined as [19]

$$NF = 1 + \frac{\sigma^2}{\langle \xi \rangle^2} \quad (5),$$

where $\langle \xi \rangle$ is the mean and σ is the standard deviation of the PHD. The NF represents the reduction of the DQE due to the statistical behavior of the avalanche process. When noise from other sources (e.g. multiplicative noise due to non-uniform sensitivity over detection area or statistical fluctuation of background exposure) is small, the DQE can be expressed as [20]

$$DQE = \frac{QE}{NF} \quad (6).$$

The goal of the Compton radiography experiments on the NIF implosions is to measure the areal density of the compressed DT fuel with sufficient accuracy. Fig. 2 shows the expected SNR versus DQE of the imaging detector, for typical implosion parameters. In order to achieve a 5% accuracy in areal density, the DQE of the detector has to be larger than 4%.

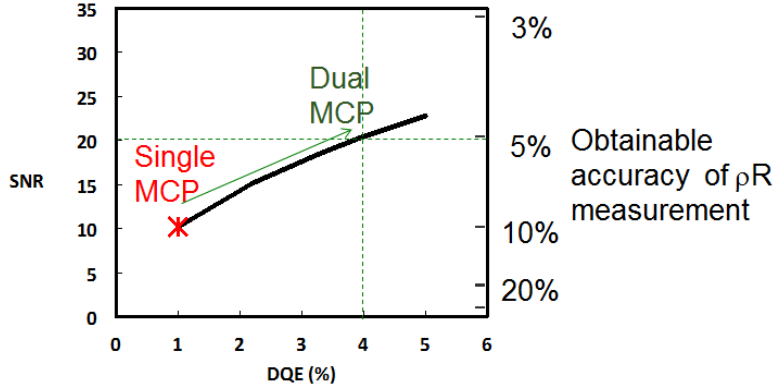


Fig. 2. Expected SNR as a function of DQE of the imaging detector. The obtainable RMS error of the inferred areal density is also shown. To achieve 5% accuracy in areal density measurement, the DQE of the detector has to reach values of 4% or better.

MEASUREMENT OF THE DQE

To demonstrate the advantage of the dual MCP configuration, we measured NF and DQE of the MCPs by using a radioactive isotope. Fig. 3 shows the experimental setup. We stacked two MCPs with a 400- μm gap between them (Table 2 shows the detail of the MCPs). Those plates were excited by 59 keV x-rays from radioactive isotope (^{241}Am , $10\mu\text{Ci}$). The low energy lines from the source were filtered by an aluminum filter (thickness: 3.88 mm). The source was located 48.5 mm from the surface of the 1st MCP. The effective area of the detector is defined by the optical aperture on the backside of the phosphor plate (aperture diameter: 12.2 mm). The x-ray flux on the effective area is 400 photons / sec. For ease of experiment, both of those MCPs are DC biased. The gap voltage V_g is set to 100V. The secondary electrons released into the pore were amplified, accelerated by the phosphor potential (3 kV), and converted to photons

in the P46 phosphor ($Y_3Al_5O_{12}:Ce$) coated on the fiber-optic face pate (FOFP). The optical output from the FOFP was detected by the photo-multiplier tube (PMT: Hamamatsu R329-02). The system is operated in x-ray photon counting regime. The multi-channel analyzer recorded the PHD. The QE was measured as the number of output pulse per incident photon. The NF was calculated from the observed standard deviation of the observed PHD.

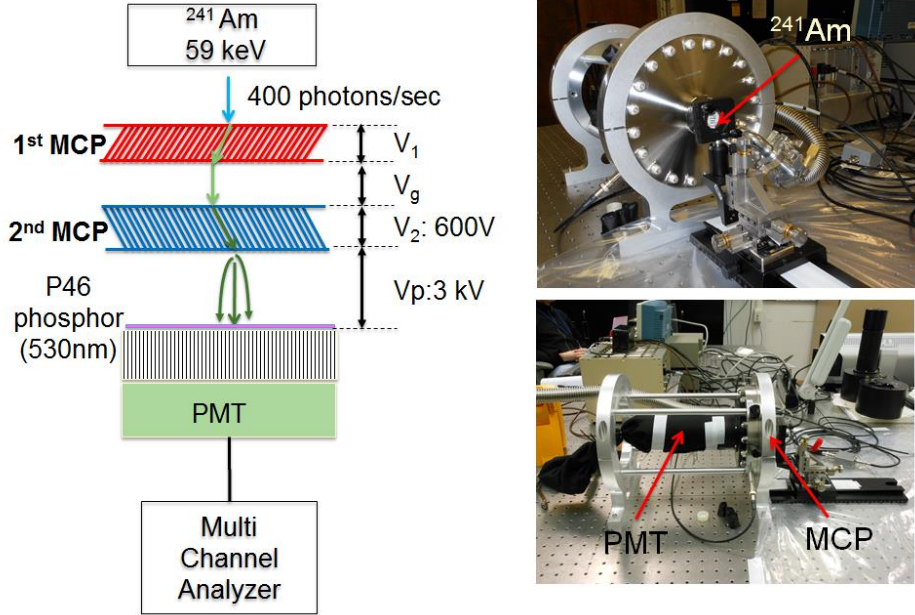


Fig. 3. Experimental setup of the DQE measurement. X-ray from ^{241}Am was used for excitation. Both the 1st and the 2nd MCP were DC biased. The system was operated in an x-ray photon counting mode. A photomultiplier tube connected to a mutual-channel analyzer recorded the amplitude of individual x-ray detection events.

Fig. 4 shows the PHDs measured in this experiment. When the 1st MCP was turned off ($V_1 = 0\text{V}$), the signal is dominated by x-ray detection events on the 2nd MCP. This PHD is almost identical to the one observed in single MCP configuration [4]. When V_1 exceed 300V, the secondary electrons produced in the 1st MCP start contributing the output. The count rate increase as a function of the V_1 because when the MCP gain is set very low, the electric field is not high enough and some avalanche streams cannot survive to the end of the pore. When V_1 is higher than 625V, the PHD starts showing tail on the high output side (with a slope of -1.0 on the log - log plot). This tail is the characteristic feature of the depth dependent gain effect [15]. Fig. 5 (a) shows the NF calculated from the observed PHDs. It is clear that the NF goes up when $V_1 > 625\text{V}$. Fig. 5 (b) shows the QE and DQE obtained in this experiment. The QE is increasing as a function of bias voltage, but maximum DQE (4.5 %) was observed when $V_1 = 625\text{V}$.

Table 2. MCPs used in the experiment

	1 st MCP	2 nd MCP
Serial No.	1719-02-22	1775-01-53
Pore diameter	10 μm	10 μm
Pore interval	12 μm	12 μm
Thickness	800 μm	460 μm
Bias angle	8deg	-8deg
Bias voltage	300 ~ 800V	600 V
Turn on voltage*	386V	504V

*The turn on voltage was estimated from test sheets provided by the manufacturer.

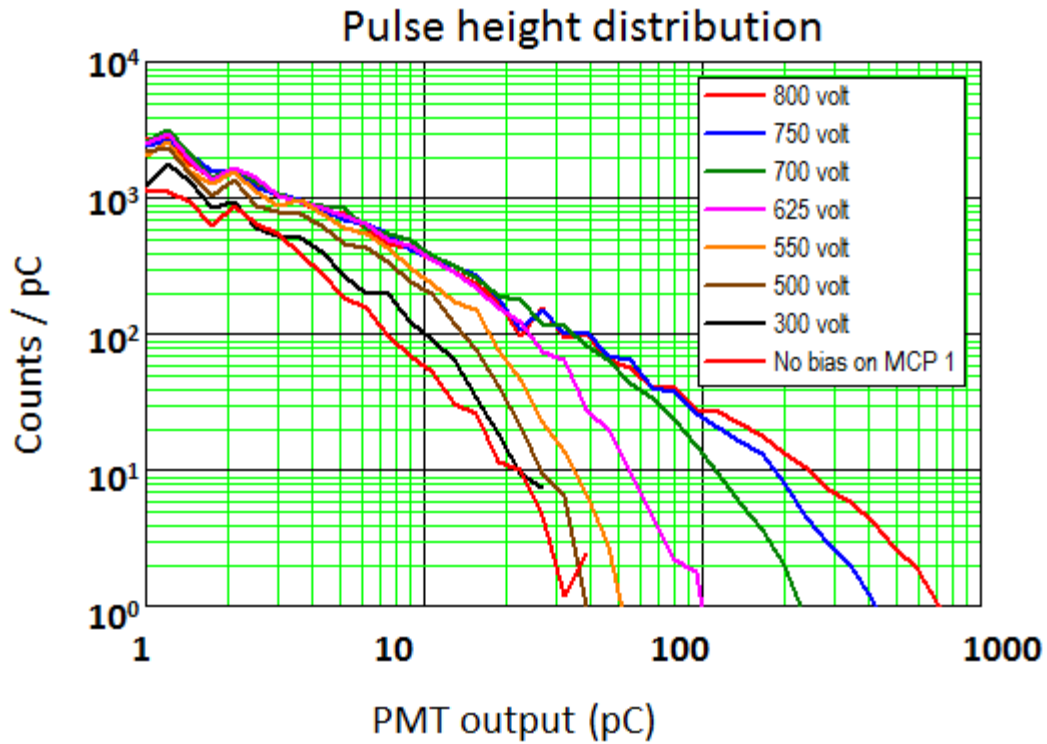


Fig. 4. Pulse height distribution obtained on the dual MCP configuration.

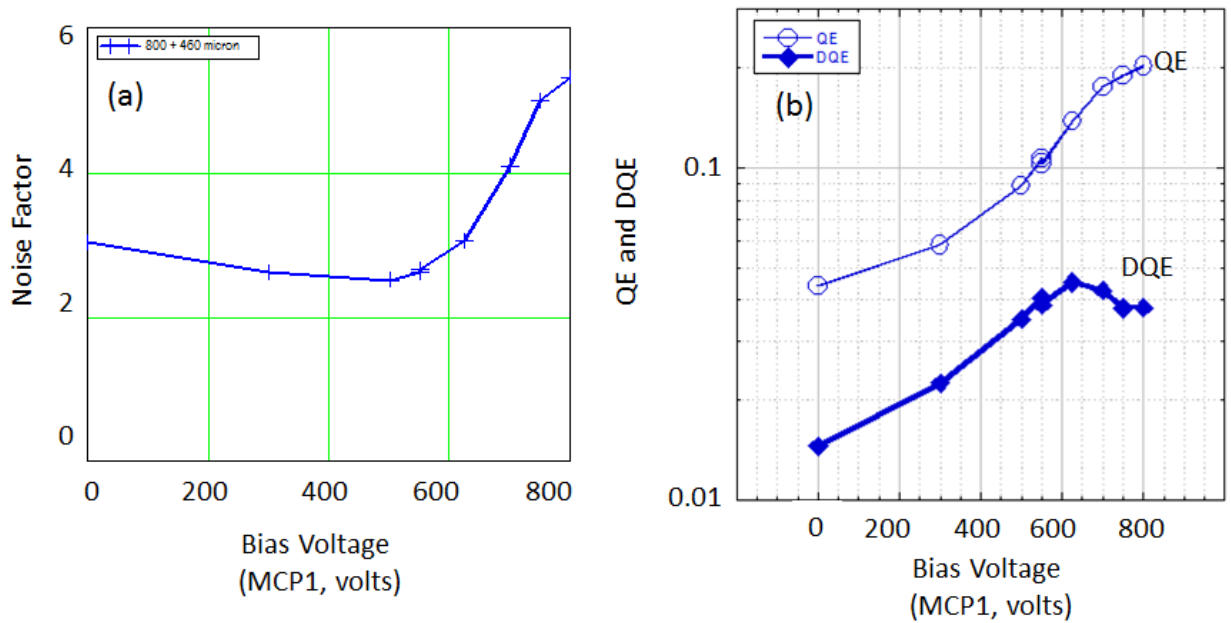


Fig. 5. Experimental results. (a) Noise factor calculated from the observed pulse height distribution. (b) Quantum efficiency and detective quantum efficiency as a function of bias voltage given to the 1st MCP.

DISCUSSION

For applications such as x-ray radiography in the Compton-scattering dominated regime[3], we require detectors with good detective efficiency at photon energies of 40keV and above. When dealing with ICF implosions, the necessity to reject long-lived sources of backgrounds demands for these detectors to be gated. By using a novel dual MCP configuration, we succeeded to greatly enhance the detective quantum efficiency of gated detectors by factors of 3x to reach values of 4.5% for 60 keV photons. We have also found that the quantum efficiency of the 1st MCP is lower than that estimated from the Monte Carlo simulation. However, the observed quantum efficiency increases with the bias voltage and asymptotically approaches to the simulated value. We believe this is due to the extinction of the electron stream in the 1st MCP when operated at very low gain. For this reason the 1st MCP has to be operated at higher-than-unity gains at the cost of accepting some increase in the noise factor due to the depth dependent gain. This problem may be suppressed by reducing the number of collisions the secondary electrons experience on the pore walls by using a 1st MCP with lower L/d aspect ratio.

ACKNOWLEDGMENT

Lawrence Livermore National Laboratory is operated by Lawrence Livermore National Security, LLC, for the U.S. Department of Energy, the National Nuclear Security Administration under Contract No. DE-AC52-07NA27344.

REFERENCES

- [1] J. D. Kilkenny, *Laser Part. Beams* 9, 49 (1991).
- [2] J. E. Bateman, et al., *Nucl. Instr. and Meth* 144, 537 (1977)
- [3] R. Tommasini, et al., *Phys. Phys. Plasmas* 18, 056309 (2011)
- [4] N. Izumi, et al., *Rev. Sci. Instrum.* 85 11D623 (2014).
- [5] G. N. Hall et al., *Rev. Sci. Instrum.* 85 11D624 (2014).
- [6] M. H. Key et al., *Phys. Rev. Lett.* 41, 1467 (1978).
- [7] H. Azechi, et al., *Appl. Phys. Lett* 37, 998 (1980)
- [8] M. Miyanaga, et al., *Appl. Phys. Lett.* 42, 160 (1983).
- [9] S. G. Glendinning, et al., *Rev. Sci. Instrum.* 70, 536 (1999).
- [10] O. L. Landen, et al., *Rev. Sci. Instrum.* 72, 627 (2001).
- [11] D. K. Bradley et al., *Optics Letters* 27 134 (2002)
- [12] F. J. Marshall et al., *Phys. Rev. Lett.* 102 (2009)
- [13] J. R. Rygg, et al., *Phys Rev. Lett.* 112, 195001 (2014).
- [14] S. E. Moran et al., *Proc. SPIE* 3173, 430–457 (1997).
- [15] K. W. Dolan, J. Chang, *Proc. SPIE* 0106, 178–188 (1997).
- [16] T. Goorley, et al., *Nuclear Technology* 180, 298 (2012).
- [17] G. E. Hill, *Adv. Electron. Electron Phys.* 40A 153 (1976).
- [18] G. Zanella, R. Zannoni, *Nucl. Instr. and Meth* A359, 474 (1995).
- [19] A. J. Guest *Acta Electron.* 14, 49 (1971).
- [20] G. Zanella, R. Zannoni, *Nucl. Instr. and Meth* A406, 93 (1998).